

Two Continuum Models for the Spreading of Myxobacteria Swarms

Angela Gallegos^a, Barbara Mazzag^b, Alex Mogilner^{a,*}

^a*Department of Mathematics, University of California, Davis, CA 95616, USA*

^b*Department of Mathematics, University of Utah, Salt Lake City, Utah 84112, USA*

Received: 11 March 2004 / Accepted: 23 March 2005 / Published online: 8 April 2006
© Society for Mathematical Biology 2006

Abstract We analyze the phenomenon of spreading of a *Myxococcus xanthus* bacterial colony on plates coated with nutrient. The bacteria spread by gliding on the surface. In the first few hours, cell growth is irrelevant to colony spread. In this case, bacteria spread through peninsular protrusions from the edge of the initial colony. We analyze the diffusion through the narrowing reticulum of cells on the surface mathematically and derive formulae for the spreading rates. On the time scale of tens of hours, effective diffusion of the bacteria, combined with cell division and growth, causes a constant linear increase in the colony's radius. Mathematical analysis and numerical solution of reaction-diffusion equations describing the bacterial and nutrient dynamics demonstrate that, in this regime, the spreading rate is proportional to the square root of both the effective diffusion coefficient and the nutrient concentration. The model predictions agree with the data on spreading rate dependence on the type of gliding motility.

Keywords Myxobacteria swarms · Gliding motility · Continuum model · Traveling wave · Colony spreading

1. Introduction

Historically, bacteria were considered solely as single-cell organisms. In recent decades, however, multicellular activities necessary for cell response to environmental changes were accepted to be common among bacteria (Shapiro, 1998). Examples of such multicellular behavior include “quorum-sensing,” auto-aggregation of chemotactic bacteria, and self-organization in bacterial colonies (Shapiro, 1998). Coordinated movements in bacterial colonies create beautiful spatio-temporal patterns that are very useful as assays for intra- and inter-cellular signaling. A good

*Corresponding author.

E-mail address: mogilner@math.ucdavis.edu (Alex Mogilner).

review of modeling of bacterial colony organization and patterns can be found in Ben-Jacob et al. (2000).

One of the most well known examples of bacterial pattern formation is the aggregation of *Escherichia coli*. This aggregation forms stable macroscopic patterns of surprising complexity when the cells, inoculated on semisolid agar, respond to gradients of chemical attractants that they themselves excrete (Berg and Budrene, 1991); similar patterns are developed in colonies of *Salmonella typhimurium* (Woodward et al., 1995). *Proteus mirabilis* colonies exhibit striking geometric regularity due to cycles of coordinated cell motion: rapid migration over a surface by groups of elongated cells encased in polymers is repeatedly followed by consolidation phases (Rauprich et al., 1996; Shapiro, 1998). Even more complex fractal shapes, typical of structures generated by diffusion-limited aggregation, are developed in *Bacillus subtilis* colonies (Ben-Jacob et al., 1994). Other examples of elaborate self-organization phenomena in bacterial colonies include the complex swarming of *Serratia liquefaciens* which wet the surface and swarm at rates increasing with time (Bees et al., 2002) as well as the “knotted-branching” swarming dynamics of spreading *Bacillus circulans* colonies (Komoto et al., 2003).

The phenomena of bacterial pattern formation attracted an uncommon amount of mathematical modeling that complements experimental studies: most of the papers cited in the previous paragraph combined theoretical and experimental approaches. We follow this tradition here by modeling quantitatively the phenomenon of spreading (often called *swarming* in biological literature) in a colony of *Myxococcus xanthus* (*M. xanthus* or *myxobacteria*). *Myxobacteria*, a common component of soil, are considered the most socially sophisticated among prokaryotes (Bray, 2002). These bacteria stay together in loose colonies pooling digestive enzymes secreted by individual cells (Shimkets and Kaiser, 1982). Under starvation conditions, myxobacteria exhibit the complex phenomena of rippling (Igoshin et al., 2001) and fruiting body formation (Jelsbak and Sogaard-Andersen, 2000), both of which have long served as paradigms of biological pattern formation.

Swarming, though nontrivial, is a simpler behavior based on the coordinated movement of many cells spreading and colonizing new areas in the presence of ample nutrients. The term “swarming” stems from observations of the feeding process, in which thousands of cells move in close proximity to each other, forming a coherent “swarm” (Shimkets and Kaiser, 1982). The swarming cells are not bound rigidly to each other and are free to move individually. However, the entire mass of cells migrates as a unit of aligned “swarmers.” We will consider a specific example of this phenomenon: a thin zone of cells is formed from a small initial colony and grows and spreads radially across a nutrient filled plate (Burchard, 1974; Kaiser and Crosby, 1983).

Motility in *Myxococcus xanthus* is controlled by two multi-gene systems. The A (adventurous) system controls gliding motility of individual, isolated cells. The S (social) system, is essential for cell movement in swarms (Spormann, 1999). Cells in swarms can move by either A-motility or S-motility or by both systems at once. Mutations in A- or S-motility genes inactivate the A- or S-system, respectively, but the cells are still motile by means of the other system (Spormann, 1999). In cases of mutations in both systems (A⁻S⁻ strains), cells are nonmotile. Myxobacteria appear to use A- or S-motility systems synergistically (Kaiser and Crosby, 1983;

Wolgemuth et al., 2002) as the motility of wild-type cells (A^+S^+) is faster than the sum of that of A^+S^- and A^-S^+ mutants. S-motility is powered by retraction of pili which appear to extend, attach to nearby cells, and then retract, pulling the cells together (Merz et al., 2000). A-motility is associated with “slime” extrusion (Wolgemuth et al., 2002). Cells appear to glide on the slime surface, reversing the direction of gliding every few minutes. The orientation of the bacteria changes slowly over hours (Shimkets and Kaiser, 1982).

Myxobacteria have been extensively modeled mathematically. Attention has focused on rippling behavior (Igoshin et al., 2001, 2004; Borner et al., 2002; Lutscher and Stevens, 2002) and aggregation (Stevens, 1995; Alber et al., 2004). Diffusion of the cells was analyzed in Koch (1999). Rigorous mathematical aspects of myxobacterial models were treated in Othmer and Stevens (1997). Some aspects of swarming behavior of myxobacteria colonies were considered in Pfister (1989), Stevens (1995), and Deutsch (1995). One of the earliest models of colony spread in a petri dish was introduced in Gray and Kirwan (1974) (see the textbook treatment of the same problem in Edelstein-Keshet (1988)). However, this model does not apply to the myxobacteria spreading as explained in Section 5. Other relevant models were considered in Newman (1980), Kawasaki et al. (1997), and Satnoianu et al. (2001).

Here we do not address questions about the biophysics of gliding, motility regulation by Mgl- and Frz-pathways and related issues (reviewed in Spormann, 1999). We do examine the relations between macroscopic spreading rates and microscopic characteristics of bacterial behavior such as gliding speed, reversal frequency and growth rate. We also attempt to answer the following important question: Can simple uncoordinated random gliding of bacteria explain the available experimental data on spreading?

The paper is organized as follows. In the next section we review the quantitative data on *M. xanthus* spreading across a nutrient filled plate (Burchard, 1974; Kaiser and Crosby, 1983). Then we make estimates of the characteristic scales of the spreading process. In Section 4 we derive the equations for spreading within the first few hours (Model A) and solve them analytically. In Section 5 we introduce the reaction-diffusion equations to describe this spreading on the time scale of tens and hundreds of hours (Model B) and solve the equations numerically. We compare the results with the experiments in Section 6 and conclude with a discussion of the results and their biological implications in Section 7. We report the phase-space analysis of the reaction-diffusion equations in the Appendix.

2. Spreading of myxobacteria

Two studies produced quantitative data on the swarming rates of *M. xanthus*: one on a long time scale of 50–250 h (Burchard, 1974) and one on a short time scale of the first 4 h (Kaiser and Crosby, 1983). The experiments in both studies were done by placing a droplet of a concentrated solution of cells on an agar-filled petri dish. The droplet was allowed to dry, forming the initial bacterial colony—a disk of cells with a radius of approximately $0.1 \mu\text{m}$. Upon drying, the thin zone of cells spread in a radially symmetric way (Fig. 1). Measurements of the radius of the colony at given time intervals demonstrate that the radius of the colony,

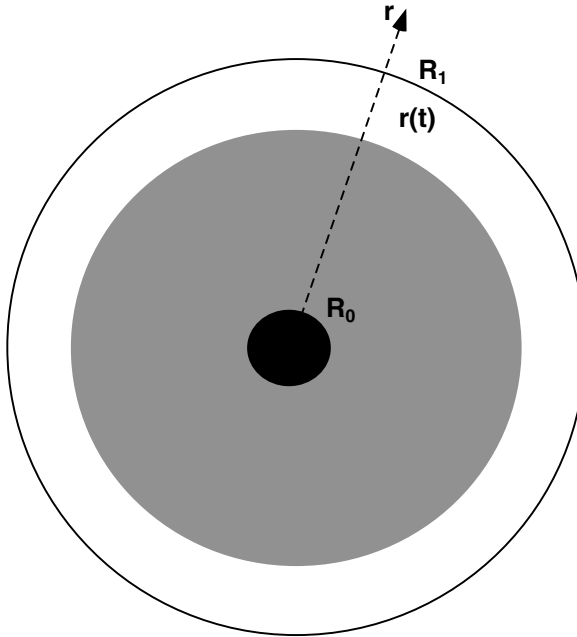


Fig. 1 Schematic top view of the radially spreading bacterial swarm on the time scale of tens of hours. Initially, the cells occupy the circular area with radius R_0 ; at time t the radius of the area covered by the cells is $r(t)$; the radius of the Petri dish is R_1 .

$r(t)$, is given by the linear function of time: $r(t) = r_0 + vt$. We call the constant v a *spreading rate*. While spreading, the bacteria consume the diffusive nutrient within the petri dish. The colonies spread with constant rate for days, until they eventually cover the entire plate and consume all available nutrient. Cell motility as well as cell division and growth contribute to the spreading rate on the long time scale (Burchard, 1974). Wild-type cells spread with the rate $3.5 \mu\text{m}/\text{min}$, while both A^+S^- , and A^-S^+ mutants' spreading rates are 2.7 times slower than that, $1.3 \mu\text{m}/\text{min}$. Burchard (1974) also observed that the spreading rates are proportional to the square root of the nutrient concentration.

Within the initial colony, the bacteria exist in a 'piled up' state, layer upon layer. Kaiser and Crosby (1983) observed that in the first few hours of spreading the bacteria first spread outward through a thin reticulum of cells (Fig. 2). More outward migration began before the newly occupied area was completely covered with cells. As the cells began to move from the smooth edge of the initial colony, where cell density was high, the front of the 'solid' colony was broken and many cell-free gaps appeared. This newly-migrating colony did not grow uniformly in all radial directions; rather, it extended finger-like appendages ('peninsulas'). Some groups of cells also broke off from the front and moved together around the colony's edge ('rafts'). Single cells were also seen to move around the colony's edge, but neither they nor the rafts travelled far away from the peninsulas and both eventually merged with the peninsulas. Inside the peninsulas individual cells were aligned in

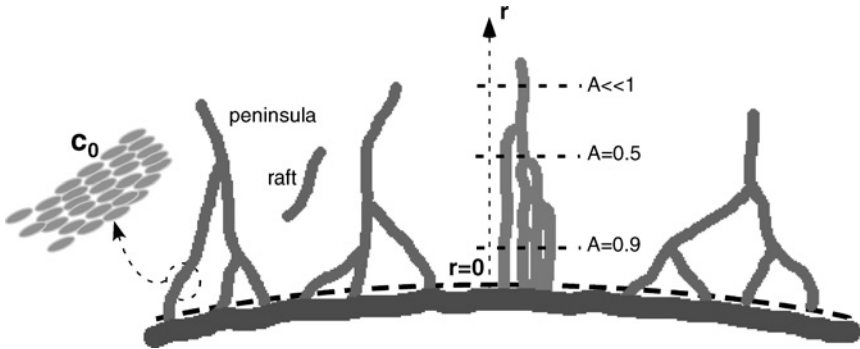


Fig. 2 Initial (first 1–3 h) spreading of aligned gliding cells (with density C_0) organized into 1D-streams (*peninsulas*). The cells develop protrusions from the edge of the initial swarm (*bold dashed line*) in the form of ‘peninsulas’ and ‘rafts.’ Merging of the peninsulas leads to the gradual decrease of the fractional area covered by motile cells away from the initial swarm edge.

the direction of their long axis (Fig. 2), vigorously gliding along this axis with direction reversing every few minutes. Open gaps between peninsulas were greater at the outer rim of the colony. Eventually, the peninsulas bent and their tips merged with the sides of other peninsulas. The open space between these peninsulas subsequently filled with cells.

Kaiser and Crosby (1983) observed that the radius of the colony increases linearly with time. In this case the radius is defined as the average distance from the colony center to the outermost peninsular tips. These results are similar to the results obtained on the long time scale. The corresponding spreading rates were of the same order of magnitude, but slower than those observed by Burchard (1974). The surprising result, however, was that the swarming rates depended on the *density of the initial colony*. The swarming rates linearly increased with initial cell density at low initial densities and saturated to constants at high densities ($1.6 \mu\text{m}/\text{min}$ for A^+S^+ and $0.6 \mu\text{m}/\text{min}$ for A^+S^- and A^-S^+ cells).

Experimental observations of the individual cells (Spormann and Kaiser, 1995; Spormann, 1999) have indicated that wild-type cells glide in the direction of their long axes with speeds varying widely between 1 and $20 \mu\text{m}/\text{min}$; the average speed is between 4 and $7 \mu\text{m}/\text{min}$. The movements of A^+S^- and A^-S^+ mutants are jerky but occur at high speeds similar to those observed in wild-type cells. Wild-type cells reverse their direction of motion every 5–7 min, so that the leading end of the cell becomes the lagging end. The mutant cells reverse their direction of motion as well, but at a frequency approximately 10-fold higher than that of wild-type cells. There is no directional bias in cell movements (Shi et al., 1996). Interestingly, the translocation velocity of individual cells varies with cell–cell distance, being slower at greater cell–cell distances and faster when the separation of cells is smaller.

Some data support the existence of chemotactic behavior in myxobacteria (Shi et al., 1993). Hence, it is not out of the question that swarming represents a chemotactic response of the bacteria to a spatial nutrient gradient (Nagai and Ikeda, 1991). Also, more complex types of cell responses, such as auto-chemotaxis and

auto-orthokinesis (increased dispersal at higher cell density), can regulate bacterial behavior (Ward et al., 1998). However, there is evidence against this taxis behavior in myxobacteria (Dworkin and Eide, 1983).

In this paper, we propose that on the long time scale of tens and hundreds of hours, traveling waves characterized by constant shape and speed develop. On the short time scale of a few hours, the bacterial growth and nutrient consumption are irrelevant. In this case, a traveling wave of bacteria diffusing through a narrowing reticulum of ‘peninsulas’ evolves. We will demonstrate that the quantitative characteristics of these traveling waves correspond to observed features of the myxobacterial spreading without additional assumptions about possible taxis behavior and cell–cell interactions.

3. Estimates of the characteristic scales of the bacterial spreading

The estimates of this section are based on the data presented in Table 1. We can estimate the effective diffusion coefficient of gliding bacteria if we note that the cells change orientation of their long axes very slowly, so that the diffusion coefficient can be estimated using the formula for 1D gliding with speed V_g and random reversals with frequency f : $D_c = V_g^2/2f$ (Berg, 1993). For wild-type cells $V_g \approx 4 - 7 \mu\text{m}/\text{min}$, and $f \approx 0.15 - 0.2/\text{min}$ (Spormann and Kaiser, 1995; Spormann, 1999), and we estimate the cell diffusion coefficient as $D_c \approx 50 - 150 \mu\text{m}^2/\text{min}$. For the mutants, the reversals are an order of magnitude more frequent, so the diffusion coefficient has to be approximately three-fold less, $\approx 15 - 50 \mu\text{m}^2/\text{min}$. We can use continuous deterministic PDE models to describe cell spreading provided that (i) we consider spatial scales longer than $V_g/f \sim 50 \mu\text{m}$; (ii) time scales longer than $1/f \sim 5 \text{min}$; (iii) cell densities much greater than a few cells per $1000 \mu\text{m}^2$; and (iv) cell densities changing slowly on the scale of $50 \mu\text{m}$. All these conditions are satisfied in the experiments that we model here (Burchard, 1974; Kaiser and Crosby, 1983).

Though there are no direct experimental data showing that the effective cell diffusion is density dependent, Kaiser and Crosby (1983) proposed a convincing argument in favor of this possibility. They suggested that when the number of cells in a certain area around a given cell increases, the random motility of this given cell increases as well. One of the simplest mathematical forms of this dependency is based on the assumption that the effective diffusion is proportional to the probability that there is at least one cell in the target area around the given cell: $\text{Prob}(\# \text{ of cells} \geq 1) = 1 - \exp(-C/C_1)$, where C is the average local cell density, and C_1 is the constant that we call the characteristic diffusion density. Following this argument, we suggest that the effective cell diffusion coefficient has the form:

$$D_c(C) = D[1 - (1 - \epsilon)\exp(-C/C_1)]. \quad (1)$$

Here D is the maximal diffusion coefficient of the cells at high density, and the dimensionless parameter ϵ is approximately the ratio of the density-independent diffusion coefficient at very small density to the maximal diffusion coefficient.

Table 1 Model parameters.

Symbol	Meaning	Value	Reference
D_h	Nutrient diffusion coefficient	$\sim 10^4 \mu\text{m}^2/\text{min}$	Woodward et al. (1995)
D	Maximal cell diffusion coefficient	$\sim 50 - 150 \mu\text{m}^2/\text{min}$	Estimated in this paper
C_0, C_1, \bar{C}	Characteristic cell densities (see text)	Unknown	—
ϵ	Ratio of density independent diffusion coefficient to maximal cell diffusion coefficient	Unknown small parameter	—
g	Nutrient uptake per cell	Unknown	—
p	Growth rate constant per nutrient concentration unit	Unknown	—
$p\bar{N}$	Characteristic cell growth rate	0.15–0.25/h	Burchard (1974)
V_g	Gliding speed	4–7 $\mu\text{m}/\text{min}$	Spormann (1999)
f	Reversal frequency	0.15–0.2/min	Spormann (1999)
ξ	Rate of peninsula merging	0.025/min	Estimated in this paper

According to the measurements of Kaiser and Crosby (1983), ϵ is a small parameter, and C_1 is much less than characteristically observed average cell densities.

The cell growth rate is $\sim 0.2/h$ (Burchard, 1974) corresponding to a characteristic growth time of 5 h. In the first few hours of spreading, the role of cell division is negligible and cell motility alone should be responsible for the observed spreading rates. Two observations about this initial stage of spreading are hard to explain. First, effective cell diffusion only cannot be responsible for the constant rate of colony spreading (Kaiser and Crosby, 1983). Indeed, diffusion (either density-independent or dependent) cannot explain the linear time dependence of colony radius increase (Murray, 1993). Second, the fact that the constant rate of spreading is observed to depend on initial colony density (Kaiser and Crosby, 1983) could suggest that there is either (i) some kind of cell memory, or (ii) a rapidly diffusing chemical signal making it possible for the bacteria to adjust their behavior to the total number of cells, similar to quorum sensing (Dockery and Keener, 2001). However, there are no data supporting these possibilities.

In the next section we propose a model explaining these observations. It is based on the following estimates, demonstrating (i) that in the first few hours only a small fraction of the bacteria leave the initial colony and spread around it, and (ii) that the cell density in the area initially occupied by the bacteria changes very little. In the experiments of Kaiser and Crosby (1983), a $7 \mu\text{l}$ droplet of solution containing 10–1000 density units of cells is deposited onto the center of a petri dish. One density unit corresponds to 4×10^6 cells/ml, so initially there are $3 \times 10^5 - 3 \times 10^7$ cells at the center. After the droplet dries, the initial radius of the bacterial colony is $R_0 \approx 100 \mu\text{m}$, and the initial area covered by the colony is $A_0 \approx 3 \times 10^4 \mu\text{m}^2$. The radius of the colony by the end of the observations (after $\sim 3\text{h}$) is $R_1 \approx 300 \mu\text{m}$; the newly covered area is $A_{\text{new}} = \pi(R_1^2 - R_0^2) \approx 2.5 \times 10^5 \mu\text{m}^2$. Kaiser and Crosby (1983) observed that, over the newly covered area, the cells are arranged in a single layer. It is rare that a second layer of cells is found atop the first layer in this region, unlike in the initial colony where tens of layers of cells are stacked on top of each other. The size of a bacterium is $\sim 4 \times 0.5 \mu\text{m}$, so the area per cell is $A_c \approx 2 \mu\text{m}^2$. Only about 25% of the surface invaded in the first few hours is covered by the reticulum of cells. Also, there is some small average separation between the neighboring cells so that $\approx 0.25 A_{\text{new}}/A_c \approx 3 \times 10^4$ cells leave the initial colony in the first few hours and spread to the originally unoccupied surface. This number of cells constitutes only 0.1–10% of the total number of cells (corresponding to 1000 to 10 density unit solutions, respectively). Therefore, the cell density at the edge of the initial colony changes very little, offering a possible explanation as to why the conditions at the edge of the colony in the first few hours do not vary with time but instead depend on the initial cell density: It is likely that the cell density at the edge of the initial colony maintains density-dependent boundary conditions at the bases of the cell streams which protrude outward. We will illustrate how the diffusion of the bacteria in these streams is effectively biased outward due to gradual merging of the streams. The resulting effective drift will explain the constant rate of increase of the colony radius.

4. Model A: Initial stage of the bacterial spreading

We model cell density dynamics in the streams of bacteria that invade the space around the initial colony. We use a 1D diffusion equation for continuous cell density. The one-dimensional character of this equation is justified by the observation that the bacteria are highly aligned along the axes of the cell streams (Fig. 2). There are gradual deviations of stream orientation from the radial direction as well as curvature effects stemming from the polar geometry of the spreading swarm. However, we neglect these effects and approximate the observed process by 1D diffusion in the radial direction (Fig. 2). In the model, r is the 1D coordinate in the outward direction; $r = 0$ corresponds to the edge of the initial colony.

The key factor in the model of the initial stage of spreading is that the fraction of the surface occupied by the cells, $A(r, t)$, decreases away from the initial colony edge. Mathematically, the model is equivalent to 1D diffusion along a narrow pipe whose cross-sectional area changes along the pipe’s axis. Specifically, if the pipe narrows monotonically, the fact that the same number of cells are passing through the narrowing area leads to an effective acceleration of the cell flux. We demonstrate below that this geometric effect causes effective cell drift that is much faster than simple diffusion at long distances.

Model variables (for both models A and B) are listed in Table 2. The conservation law for cell number in the described geometry has the form (Edelstein-Keshet, 1988):

$$\frac{\partial[A(r, t)C(r, t)]}{\partial t} = -\frac{\partial J(r, t)}{\partial r}, \quad J(r, t) = -A(r, t)D_c(C(r, t))\frac{\partial C(r, t)}{\partial r}.$$

Here J represents cell flux; we assume that only effective diffusion is responsible for the flux. The fraction of the surface occupied by the cells, $A(r, t)$, is a dimensionless quantity. $A = 1$ if the whole surface is covered with the cells, and $A = 0$ for the empty surface. Substituting the diffusive flux into the conservation law, we obtain the diffusion equation:

$$\frac{\partial[AC]}{\partial t} = \frac{\partial}{\partial r} \left[AD_c \frac{\partial C}{\partial r} \right]. \tag{2}$$

Table 2 Model variables.

Symbol	Meaning	Units
t	Time	min or h
r	Radius of the bacterial colony	μm or mm
$c(r, t)$	Cell density	Dimensionless units
$n(r, t)$	Nutrient concentration	Dimensionless units
$A(r, t)$	Fraction of the surface occupied by the cell	Dimensionless
$P(r, t)$	Density of the peninsula tips	$\#/\mu\text{m}^2$
v	Traveling wave speed	Dimensionless units, or $\mu\text{m}/\text{min}$

Using the product rule for differentiation as well as the formula for the derivative of a logarithmic function, Eq. (2) can be rewritten in the following form:

$$\frac{\partial C}{\partial t} = \frac{\partial}{\partial r} \left[D_c \frac{\partial C}{\partial r} \right] - \left[D_c \frac{\partial(-\ln A)}{\partial r} \right] \frac{\partial C}{\partial r} - \left[\frac{\partial(\ln A)}{\partial t} \right] C. \quad (3)$$

The structure of the right hand side of Eq. (3) suggests the following helpful interpretation. The first term on the right hand side accounts for simple diffusion. The second term describes the effective drift which has a velocity proportional to the rate of decrease (with respect to distance) of the area occupied by the cells. The narrowing of the area through which the cells have to squeeze biases the diffusion outward, causing this effective drift. The third term is responsible for a sink effect in cell density which occurs proportionally to the rate of increase (with respect to time) of the area occupied by the cells. An increase in the area occupied by the cells over time means the cells have spread to a larger area, essentially decreasing their density.

Equation (3) for the cell density has to be complemented with an equation for the fraction of the surface occupied by the cells, $A(r, t)$. We derive the latter assuming that the tips of the ‘peninsulas’ (streams of cells) extend in the radial direction with constant speed v , and that the tips merge with constant rate ξ . Accordingly, the density of the peninsula tips, $P(r, t)$, can be quantified as:

$$\frac{\partial P}{\partial t} = -v \frac{\partial P}{\partial r} - \xi P. \quad (4)$$

It is easy to check that this equation has the following solution in the form of the decaying traveling pulse:

$$P(r, t) = P_0 e^{-\xi t} \delta(r - vt), \quad (5)$$

where P_0 is the normalization constant, and $\delta(r)$ is the initial delta-like spatial distribution of the tips. We neglect the emergence of new tips from the sides of existent peninsulas. We also assume that all tips emerge from the edge of the initial colony almost simultaneously at the beginning of spreading and that no tips emerge later in time.

When tips merge we make the width of the single peninsula twice less than the sum of the width of the two peninsulas before merging. Given this assumption and assuming a constant width for the peninsulas, the fraction of the surface occupied by the cells at coordinate r and time t can be found:

$$A(r, t) = A_0 \int_0^t P(r, \tau) d\tau = H(r - vt) e^{-r/l}. \quad (6)$$

Here $l = v/\xi$, and A_0 is a normalization constant. We assume that $A(r = 0, t = 0) = 1$, meaning that, at the edge of the original colony, the whole surface is

covered by the spreading bacteria. In this equation, $H(\cdot)$ is the unit step function which emerges after integration in formula (6) if $\delta(r)$ in expression (5) is exactly the delta-function. Realistically, $\delta(r)$ is a smooth function with compact support on a small interval so that $H(\cdot)$ is a smooth step-like function. For simplicity, we use the exact unit step function: $H(z) = 1$ if $z > 0$, and $H(z) = 0$ if $z < 0$.

The model predicts that there are no cells on the surface for $r > vt$ (i.e., $A(r, t) = 0$ at $r > vt$). After the peninsula tips propagate over the surface, the fraction of the surface occupied by the cells depends on distance but is constant in time: $A(r, t) = \exp[-r/l]$ for $r < vt$ (Fig. 3). (Eventually, the whole surface is covered by bacteria, but we assume that this happens on a longer time scale and do not model it explicitly. For longer times, the A -profile might also be modeled to converge to a stationary travelling front, too.) For $r < vt$,

$$\frac{\partial(\ln A)}{\partial t} = 0, \quad \frac{\partial(-\ln A)}{\partial r} = \frac{1}{l},$$

and Eq. (3) simplifies to the form:

$$\frac{\partial C}{\partial t} = \frac{\partial}{\partial r} \left[D_c \frac{\partial C}{\partial r} \right] - \frac{D_c}{l} \frac{\partial C}{\partial r}. \tag{7}$$

The second term in (7) can be re-written as:

$$\frac{D_c(C)}{l} \frac{\partial C}{\partial r} = \frac{\partial}{\partial r} [V(C)C], \quad V(C)x = \frac{1}{lC} \int D_c(C) dC.$$

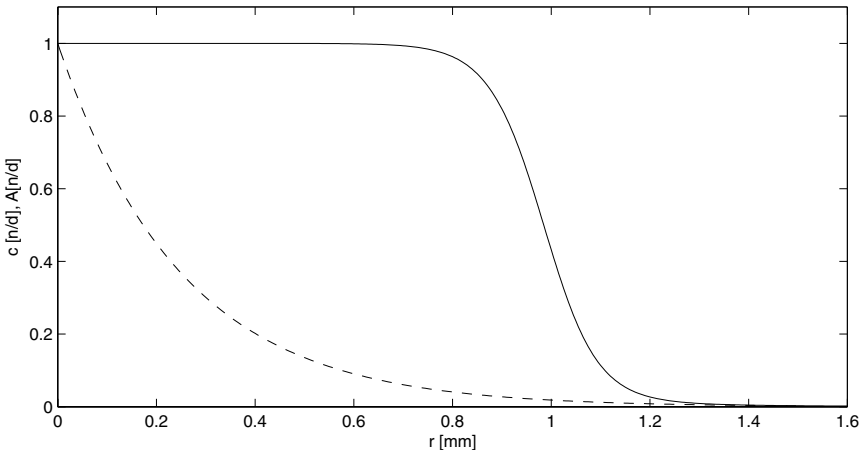


Fig. 3 Cell density (solid; numerical solution of (11)) along a protrusion from the edge of the bacterial colony, and the fraction of the surface occupied by the cells (dashed, Eq. (6)) at some time after the spreading starts and the traveling wave develops.

Integrating and choosing integration constant so that $V(C)$ is finite as $C \rightarrow 0$,

$$V(C) = \frac{D}{l} \left[1 - (1 - \epsilon) \frac{C_1}{C} \left(1 - \exp\left(-\frac{C}{C_1}\right) \right) \right]. \tag{8}$$

Effectively, the bacteria undergo outward drift with rate $V(C)$ that is of the order of (and has similar density dependence to) the diffusion coefficient, D , divided by the characteristic distance, l , over which the number of peninsulas decreases significantly.

We are looking for the traveling wave solution of Eq. (7):

$$C(r, t) = C(z) = C(r - vt), \quad -v \frac{dC}{dxz} = \frac{d}{dz} \left[D_c \frac{dxC}{dz} \right] - \frac{\partial}{\partial z} [V(C)C]. \tag{9}$$

The shape of the traveling wave depends on the nature of the boundary conditions at the front and back of it. In our case, the back of the wave is characterized by the condition at the edge of the initial colony ($r = 0$). At this edge we assume that there is a rapid exchange of cells, with a high constant transition rate of bacteria from the edges of the initial colony into the peninsular protrusions as well as a small rate of transition from the peninsular bases back into the initial colony. The former rate can be assumed to be constant because, as we demonstrated above, the total number of bacteria in the initial colony changes very little in the first few hours of spreading. The latter rate can be assumed to be proportional to the local density at the base of the peninsula. Due to this proportionality, *a constant cell density is maintained at the bases of peninsulas protruding outward from the initial colony edge*. We denote this density as C_0 . This boundary density is likely to be an increasing function of the initial colony density.

Let us use the value C_0 as the density scale, l^2/D as the time scale, and introduce the dimensionless quantities $c = C/C_0$, $c^* = C_1/C_0$, and $x = z/l$. Thus, we obtain the equation for the density profile:

$$\frac{d}{dx} \left[\tilde{D}(c) \frac{dc}{dx} + (v - \tilde{V}(c))c \right] = 0, \tag{10}$$

$$\tilde{D} = 1 - (1 - \epsilon) \exp(-c/c^*), \quad \tilde{V} = 1 - (1 - \epsilon)(c^*/c)(1 - \exp(-c/c^*)).$$

Integrating (10) once and using boundary conditions ahead of the front ($x \rightarrow \infty, c \rightarrow 0, dc/dx \rightarrow 0$), we find that the integration constant is zero, and $\tilde{D}(dc/dx) + (v - \tilde{V})c = 0$. Using boundary conditions behind the front ($x \rightarrow -\infty, c \rightarrow 1, dc/dx \rightarrow 0$), we find that $v = \tilde{V}(1)$, and:

$$\frac{dc}{dx} = -\frac{\tilde{V}(1) - \tilde{V}(c)}{\tilde{D}(c)} xc. \tag{11}$$

The corresponding shape of the traveling wave obtained by solving (11) numerically is shown in Fig. 3: the cell density is constant along the stream and decreases

to zero at the tip over the characteristic distance l . To find the wave's velocity, note that in dimensional variables, $v = (D/l)\tilde{V}(1) = (D\xi/v)\tilde{V}(1)$, and:

$$v(C_0) = \sqrt{D\xi} \left[1 - (1 - \epsilon) \frac{C_1}{C_0} \left(1 - \exp\left(-\frac{C_0}{C_1}\right) \right) \right]^{1/2}. \tag{12}$$

5. Model B: Bacterial spreading on the long time scale

On the time scale of tens and hundreds of hours both cell movement and growth become important. We use a reaction-diffusion equations approach (Edelstein-Keshet, 1988; Murray, 1993) to describe the system with radially symmetric cell density, $C(r, t)$, and nutrient concentration, $N(r, t)$. Rigorously speaking, the densities can also be functions of the angle in the polar coordinate system where the origin is located at the center of the colony. However, we neglect this angle dependence by assuming radial symmetry for both the cell and nutrient distributions. This assumption is based firstly on experimental observations, and secondly on proved stability for the radially symmetric solutions of the equations introduced below (for review, see (Ben-Jacob et al., 2000)).

We describe the dynamics of cell density and nutrient concentration by the following system of equations:

$$\frac{\partial C}{\partial t} = \frac{\partial}{\partial r} \left[D_c(C) \frac{\partial C}{\partial r} \right] + \frac{1}{r} D_c(C) \frac{\partial C}{\partial r} + pCN, \tag{13}$$

$$\frac{\partial N}{\partial t} = D_n \left[\frac{\partial^2 N}{\partial r^2} + \frac{1}{r} \frac{\partial N}{\partial r} \right] - g pCN. \tag{14}$$

The first two terms on the right hand sides of (13, 14) are responsible for the radial diffusion of cells and of nutrient. D_n is the constant diffusion coefficient of the nutrient. The third term on the right hand side of (13) describes exponential growth of cell density with growth rate pN , proportional to the nutrient concentration. The parameter p represents the growth rate per nutrient concentration unit. Cell growth slows down as the nutrient is depleted, stopping when $N = 0$. The third term on the right hand side of (14) describes the corresponding nutrient depletion. In this case the parameter g represents the constant nutrient uptake per new cell (in other words, $g pCN$ units of nutrient are consumed per unit time, while pCN new cells appear). Note that the model is based on the assumption that nutrient concentration affects cell behavior only through its effect on cell growth and not its effect on cell gliding speed (Burchard, 1974). Also, little is known about the functional form for the nutrient consumption (Rosenberg et al., 1977). For simplicity, we assume a constant consumption rate per cell in the model.

To cast the model in nondimensional terms, we choose the initial inverse cell growth rate, $T = 1/(p\bar{N}) \sim 5$ h, as the time scale. Here \bar{N} is the constant initial nutrient concentration. For the spatial scale we choose $L = \sqrt{D_n T} \sim 0.2$ mm—the characteristic distance of nutrient diffusion over the characteristic time scale. The scale of velocity then follows: $L/T = \sqrt{D_n p \bar{N}} \sim 10$ μ m/min. The natural scale of nutrient concentration is its initial value, \bar{N} . As g units of nutrient are

consumed per new cell, the appropriate scale of cell density is $\bar{C} = \bar{N}/g$. Introducing the nondimensional dependent and independent variables, $c = C/\bar{C}$, $n = N/\bar{N}$ and $t' = t/T$, $r' = r/L$, respectively (and dropping the prime notations for convenience; now $c^* = C_1/\bar{C}$), we arrive at the following nondimensional system of model equations:

$$\frac{\partial c}{\partial t} = \frac{D}{D_n} \frac{\partial}{\partial r} \left[\bar{D}(c) \frac{\partial c}{\partial r} \right] + \frac{D}{D_n r} \bar{D}(c) \frac{\partial c}{\partial r} + cn, \quad (15)$$

$$\frac{\partial n}{\partial t} = \left[\frac{\partial^2 n}{\partial r^2} + \frac{1}{r} \frac{\partial n}{\partial r} \right] - cn. \quad (16)$$

Effective cell diffusion estimated below is two orders of magnitude smaller than the known order of magnitude of nutrient diffusion in agar (Table 1), so $D/D_n \sim 0.01 \ll 1$ is a small parameter.

In the limit of the large colony radius, which is valid on the relevant time scale (in experiments described in Burchard (1974), $r \sim 10$ mm, and $r/L \sim 100$), the second terms in the square brackets in Eqs. (15, 16) can be neglected in comparison with the corresponding first terms (Murray, 1993), and the model system is reduced to the effective one-dimensional problem:

$$\frac{\partial c}{\partial t} = \frac{D}{D_n} \frac{\partial}{\partial r} \left[\bar{D}(c) \frac{\partial c}{\partial r} \right] + cn, \quad (17)$$

$$\frac{\partial n}{\partial t} = \frac{\partial^2 n}{\partial r^2} - cn. \quad (18)$$

The analysis of the similar system in Gray and Kirwan (1974) (they considered a density-independent cell diffusion) was based on neglecting cell diffusion altogether based on the strong inequality $D/D_n \ll 1$: $\partial c/\partial t = cn$, $\partial n/\partial t = \partial^2 n/\partial r^2 - cn$. It was shown that, in this limit, there exists a unique stable traveling wave solution with corresponding speed $v = \mu\sqrt{D_n p \bar{N}}$, $\mu \sim 1$. In this case, the spreading rate is independent of the bacterial diffusion coefficient, which fails to explain the dependence of the spreading rate on bacterial motility (Burchard, 1974). However, the analysis of Gray and Kirwan (1974) is valid for so-called *kinetic* traveling waves (Fife, 1979), where the bacterial spread is limited by cell growth and nutrient diffusion. Such traveling waves evolve from an initial condition where cells are spread across the whole petri dish, with density decreasing rapidly away from the center (Billingham and Needham, 1991a,b). This initial condition is biologically unrealistic in the experimental context (Burchard, 1974; Kaiser and Crosby, 1983) where the bacteria are concentrated initially in a finite disc in the center of the petri dish. Mathematically, this experimentally relevant case corresponds to a stable traveling wave evolving from an initial cell density with compact support. Billingham and Needham (1991a,b) showed rigorously for Eqs. (17, 18) *with density-independent diffusion* that for such initial conditions a stable traveling wave evolved with dimensionless velocity $v = 2\sqrt{D/D_n}$.

To investigate the swarming behavior indicated by the full radially symmetric and density dependent diffusion model system, we solved Eqs. (15, 16)

numerically. We used the explicit Forward-Time Centered-Space method (Garcia, 2000) and solved the model equations on a desktop computer using MatlabTM. In the simulations, we used a spatial interval equal to 100 length units with no flux boundary conditions at either end. Space was discretized equidistantly with 10 grid points per unit length. The equations were integrated with a time step equal to 0.001 units of time, ensuring the numerical stability of the method. The simulations ran for a few tens of time units corresponding to 500 h of real time. In all simulations, the initial nondimensional nutrient concentration $n(r, 0) = 1$ was constant across the space interval.

We first ran the simulations with the cell density equal to zero across the space, except at the left endpoint of the interval ($r = 0$) where it was equal to 1. Figure 4 shows the cell densities and nutrient concentrations at consecutive equidistant times. The values $D/D_n = 0.2$, $\epsilon = 0.05$, and $c^* = 0.03$ correspond to these simulations. The figure illustrates that at first the cell density builds up near the origin, develops a steep gradient at the edge of the swarm, and starts to spread outward. Then a constant shape at the front of the colony develops and starts to propagate with constant speed. After that, the cell density behind the front remains constant and equal to 1, while decaying in time at the colony center ($r = 0$) (Fig. 4). Meanwhile, the nutrient is consumed in the region invaded by the cells. The gradient of the nutrient concentration develops opposite to that of the cell density. The shape of the trailing edge of the nutrient concentration is steady and propagates outward synchronously with cell density.

To investigate the traveling wave speed dependence on parameters D/D_n , ϵ , and c^* , we ran the simulations at different values of these parameters (note that biologically relevant values for each of these parameters are small). The numerical results (Fig. 5A) demonstrate that the dimensionless traveling wave speed is proportional to the square root of the ratio D/D_n . Furthermore, the traveling wave speed depends weakly on small parameters ϵ and c^* (Fig. 5B, C). The numerical analysis suggests that the dimensional traveling wave speed can be written in the form:

$$v = \mu(\epsilon, c^*)\sqrt{Dp\bar{N}}, \quad \mu(\epsilon, c^*) \sim 1. \quad (19)$$

Phase plane analysis (Appendix) supports the conclusions from the numerical analysis.

6. Comparison of the theoretical results and experimental data

The main conclusions of our paper stem from Eqs. (12, 19). These equations predict that both on the short (less than 5 h, (12)) and long (more than 10 h, (19)) time scales the spreading rate is proportional to the square root of the maximal (at saturation at high density) diffusion coefficient. Both Burchard (1974), and Kaiser and Crosby (1983) observed that colonies of nonmotile mutants A^-S^- do not spread, in agreement with our theory. According to the estimate in Section 3, the diffusion coefficient of the A^+S^- and A^-S^+ mutants is an order of magnitude less than

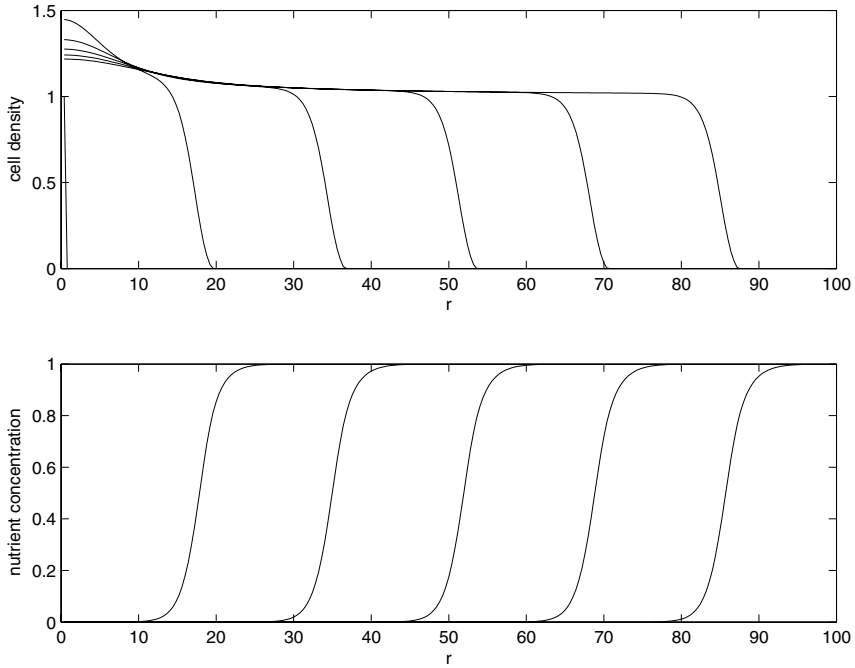


Fig. 4 Results of numerical simulations of the reaction-diffusion eqs. (15, 16) in the polar coordinate system describing cell and nutrient dynamics. Both densities and the distance are in nondimensional units. The model parameters are $D/D_n = 0.2$, $\epsilon = 0.05$, and $c^* = 0.03$. The densities are plotted at equal time intervals (at $t = .02, 30, 60, 90, 120, 150$ time units).

that of the wild-type cells. Therefore, the model predicts that the spreading rate of the mutants has to be roughly three times less than that of wild-type cells. Experimental values for mutant spreading speeds on the short time scale, $0.6 \mu\text{m}/\text{min}$, (Kaiser and Crosby, 1983), are indeed approximately 2.7-fold smaller than the wild-type spreading speed of $1.6 \mu\text{m}/\text{min}$ (Kaiser and Crosby, 1983), confirming this prediction. Remarkably, the measured ratio of the wild-type spreading speed ($3.5 \mu\text{m}/\text{min}$) to that of the mutants ($1.3 \mu\text{m}/\text{min}$) on the long time scale (Burchard, 1974) is also 2.7, which indicates the model's validity.

Theoretically, we estimate the value of the spreading rate on the long time scale using the estimate for the cell diffusion coefficient $D \sim 100 \mu\text{m}^2/\text{min}$ and the characteristic cell growth rate $p\bar{N} \sim 0.25/\text{h}$. Thus, $v \sim \sqrt{Dp\bar{N}} \sim 1 \mu\text{m}/\text{min}$, which compares well with the experimentally observed range of speed: $1\text{--}4 \mu\text{m}/\text{min}$ (Burchard, 1974).

On the short time scale, we can estimate the parameter ξ knowing that the swarming rate of the wild-type cells at saturation is $v \approx 1.6 \mu\text{m}/\text{min}$ (Kaiser and Crosby, 1983). Using the estimated value of the diffusion coefficient, $D \sim 100 \mu\text{m}^2/\text{min}$, we estimate $\xi \sim v^2/D \sim 0.025/\text{min}$. Thus, the model predicts that the individual peninsulas exist for $\sim 1/\xi = 40$ min. The corresponding average length of the peninsulas is $v/\xi \sim 60 \mu\text{m}$ and is equal to the characteristic distance on which

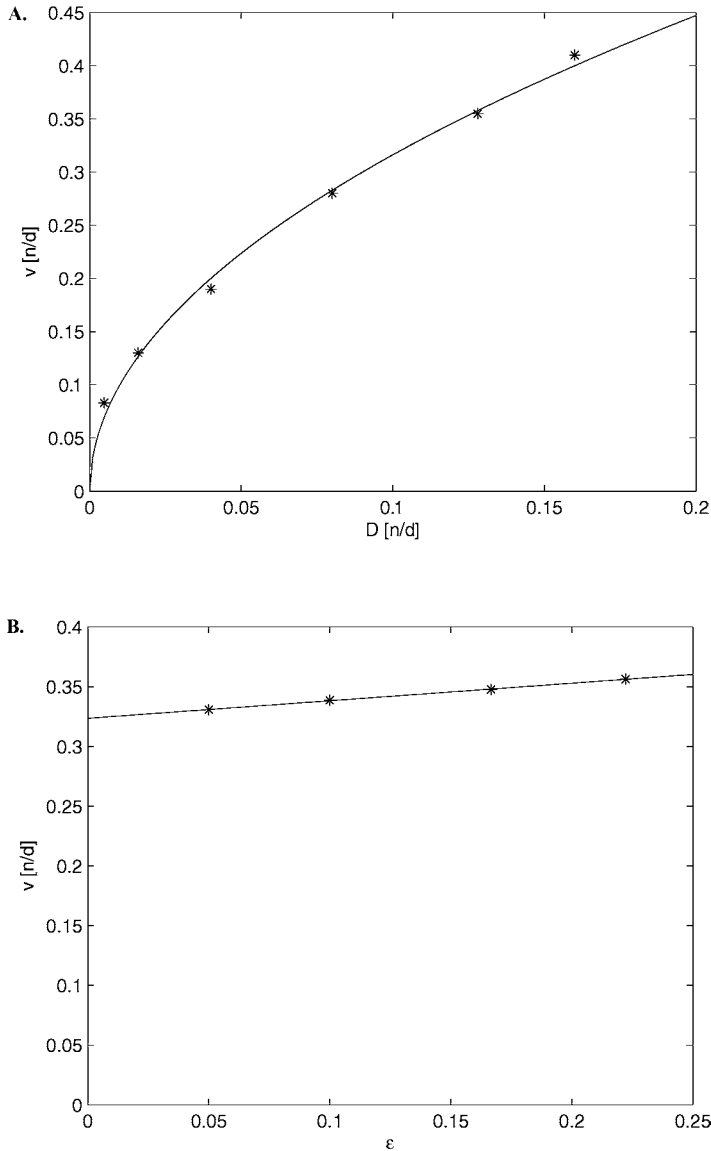


Fig. 5 A. Spreading rate dependence on the cell diffusion coefficient (units of D_n), obtained numerically from solving (15, 16) and shown with stars, is fitted well by the equation $v \approx \sqrt{D}$. The model parameters are $\epsilon = 0.06$, $c^* = 0.1$. B. Spreading rate weak dependence on the ratio of density-independent to density-dependent parts of the diffusion coefficient (nondimensional parameter ϵ), obtained numerically from solving (15, 16) and shown with stars, is fitted well by the equation $v \approx 0.32 + 0.16\epsilon$. The model parameters are $D/D_n = 0.1$, $c^* = 0.1$. C. Spreading rate weak dependence on the ratio of characteristic diffusion density to average cell density (nondimensional parameter c^*), obtained numerically from solving (15, 16) and shown with stars, is fitted well by the equation $v \approx 0.21/(c^*)^{1/5}$. The model parameters are $D/D_n = 0.1$, $\epsilon = 0.1$.

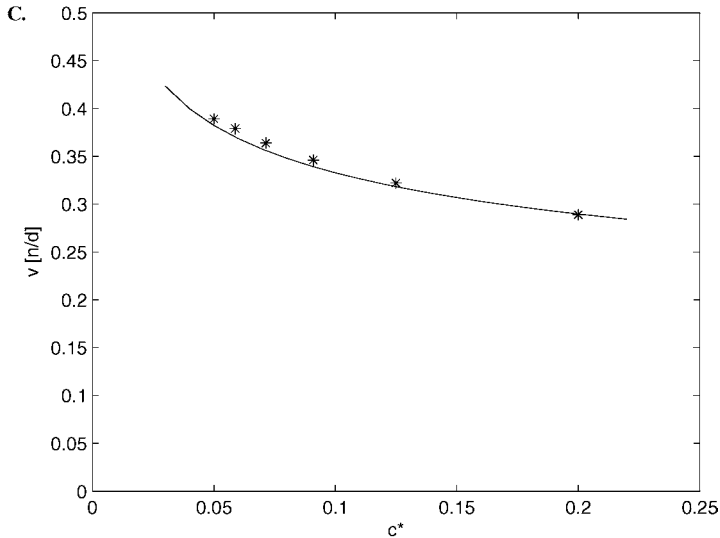


Fig. 5 continued

the area covered by the cells diminishes significantly. Using these calculations, we estimate the total area covered by the reticulum of cells as $\sim 25\%$. The average estimated length of the peninsulas seems to agree well with that gleaned from published micrographs (Kaiser and Crosby, 1983).

Another important conclusion from Eq. (19) is that on the long time scale the spreading rate is proportional to the square root of the nutrient concentration, as observed (Burchard, 1974). Also, we predict that the rate of spreading does not depend on the nutrient diffusion coefficient.

Finally, we have plotted the dependence of the spreading velocity on the cell density at the edge of the colony on the short time scale (Fig. 6). Qualitatively, this dependence compares well with that observed by Kaiser and Crosby (1983), assuming that C_0 is an increasing function of the initial cell density used in the experiments. Quantitative comparison is impossible because the exact dependence of C_0 on the initial cell density is unknown. However, comparison with experimental results (Kaiser and Crosby, 1983) is sufficient to see that the parameter ϵ is small, ~ 0.1 , and that the parameter c^* in Eq. (19) is also small, ~ 0.1 .

7. Discussion

In this paper we have proposed two mathematical models to describe the spreading of myxobacteria on both short (a few hours) and long (tens and hundreds of hours) time scales. The long time scale model (B) consists of two reaction-diffusion equations, describing diffusing, growing cells as well as diffusing, consumed nutrient. A similar model was described earlier (Gray and Kirwan, 1974)

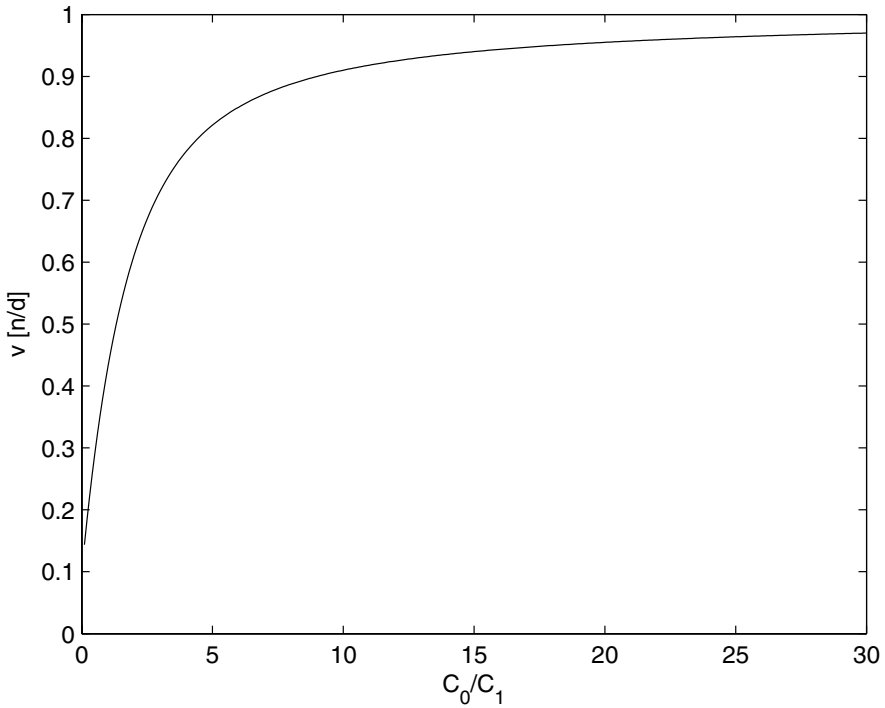


Fig. 6 Spreading rate (nondimensional, in units of $\sqrt{D\xi}$) as a function of the nondimensional cell density (C_0/C_1) predicted by (12) at $\epsilon = 0.1$.

but it considered a traveling wave solution corresponding to a spreading rate that depended on the nutrient diffusion coefficient but not the cell diffusion coefficient; this is unbiological. A biologically relevant solution for the same model was found in Billingham and Needham (1991a,b) but for a constant diffusion coefficient and applied to different problems. For density-dependent cell diffusion, we demonstrated the existence of a biologically relevant traveling wave solution whose speed is independent of the nutrient diffusion coefficient and proportional to the square roots of both the cell diffusion coefficient and growth rate. We estimated the effective cell diffusion coefficients for both wild-type cells and mutants using the data from Spormann and Kaiser (1995) and demonstrated that the theoretical estimates of the spreading rates compare well with the measurements of Burchard (1974). The model explains successfully the fact that the mutants’ spreading rates are 2–3-fold less than those of the wild-type cells. The model prediction that the spreading rate is proportional to the square root of the initial nutrient concentration agrees with the corresponding observations (Burchard, 1974). The model also makes predictions that can be tested in future experiments, such as (i) the independence of the spreading rate from the nutrient diffusion coefficient and (ii) the dependence of the spreading colony density being proportional to the initial nutrient concentration.

We demonstrated that within a few hours after the onset of spreading, only a small fraction of bacteria leaves the initial colony. Thus, we have hypothesized that the initial cell density at the original colony edge maintains a boundary condition for a few hours that determines spreading rate. The short time scale model consists of a cell diffusion equation on the dynamic reticulum as well as equations describing the dynamics of this reticulum. The model assumes that the tips of the peninsulas protruding from the colony edges merge with constant rate. The model analysis demonstrates the existence of a traveling wave solution for the decreasing number of peninsulas and cells undergoing effective outward diffusion through this narrowing reticulum. The model analysis also demonstrates that if the characteristic lifetime of individual peninsulas is on the order of 40 min, then the observed spreading rates for both wild-type cells and mutants (Kaiser and Crosby, 1983) agrees well with our estimates. The model makes the testable prediction that the fraction of the area occupied by the cells decreases exponentially in the outward direction on a spatial scale of $\sim 60 \mu\text{m}$. Kaiser and Crosby (1983) suggested that the spreading rates' density dependence is not due to competition for space or nutrient, but rather to interactions between the cells. In this paper we demonstrated that all the available quantitative data on the spreading rates can be explained by assuming simple uncoordinated gliding and random reversals of myxobacteria.

The model does not address the important question about the nature of the synergism between the two motility systems discussed in the Introduction. Corresponding modeling would require more elaborate quantitative analysis of microscopic data, some of which, such as the correlation between cell movements, is missing. In the future, it would be important to measure accurately the statistics of individual cell movements, as well as the fraction of the area at the colony edge occupied by cells. We also did not incorporate into the model the fact that the cells are fully motile at the periphery of the colony while nonmotile in the older, interior region where nutrient is depleted. Numerical simulations not reported here have shown that these effects do not change the model conclusions qualitatively. Most importantly, we oversimplified the dynamics of the formation of the cell reticulum at the edges of the colony: in reality, new peninsulas emerge from the sides of old ones and cells fill the gaps between the peninsulas. Taking these particular dynamics into account could make the model more interesting and adequate and is worth doing in the future. Also, a more comprehensive model that addresses the spreading at intermediate times as well as the colony's dynamics on smaller scales of hundreds of microns is still pending.

The model can explain why *mgl*-mutants do not spread (Spormann and Kaiser, 1999). These mutants glide with twice-slower speeds and reverse directions at frequencies more than an order of magnitude higher than those of wild-type cells (Spormann and Kaiser, 1999). The explanation would be that the effective diffusion coefficient for these cells is very small as it is proportional to the square of the gliding speed and inversely proportional to the reversal frequency. However, the same argument fails to explain the ineffective spreading of the low reversal frequency *frz*-mutants (Shi et al., 1993) whose time between reversals is greater than 120 min. According to our theory, these mutants diffuse and swarm very rapidly. This problem (along with other potential complications) indicates that our simplified models miss some important effects stemming from nontrivial

cell–cell interactions. Despite this, our model is an important initial step in the theoretical understanding of myxobacteria swarming. Future, more realistic modeling would require concerted experimental and theoretical effort.

Acknowledgements

A. M. and A. G. were supported by a UCD Chancellor’s fellowship, NSF Award DMS-0073828 and NIH GLUE grant ‘Cell Migration Consortium’ NIGMS U54 GM64346. A. G. and B. M. were supported by RTG-NSF-DBI-9602226 grant and VIGRE NSF grant to Math Department at UCD. The authors are grateful to O. Igoshin, G. Oster, D. Kaiser, A. Spormann, and D. Zusman for fruitful discussions and to anonymous reviewers for useful suggestions.

Appendix: Phase-space analysis of the traveling wave speed

Model Eqs. (17) and (18) possess a continuous family of traveling wave solutions where $z = r - vt$, $c(z) = c(r - vt)$, and $n(z) = n(r - vt)$. Substituting these expressions into (17, 18), we obtain the equations for the shape of the traveling wave:

$$-v \frac{dc}{dz} = \frac{D}{D_n} \frac{d}{dz} \left[\tilde{D}(c) \frac{dc}{dz} \right] + cn, \tag{A.1}$$

$$-v \frac{dn}{dz} = \frac{d^2n}{dz^2} - cn. \tag{A.2}$$

For these equations, the uniform solutions $c = 1, n = 0$ and $c = 0, n = 1$ are, respectively, stable and unstable. There exists a one-parameter family, $c_v(z), n_v(z)$, of traveling wave solutions (indexed by their velocity v) with $c_v(z)$ decreasing and $n_v(z)$ increasing, that is, $c_v(z) \rightarrow 1$ and $n_v(z) \rightarrow 0$ as $z \rightarrow -\infty$ and $c_v(z) \rightarrow 0$ and $n_v(z) \rightarrow 1$ as $z \rightarrow +\infty$. The analytic expressions for $c_v(z), n_v(z)$ are not known, but one can determine the range of velocities v for which solutions of this type exist.

Adding Eqs. (20) and (21) gives:

$$\frac{D}{D_n} \frac{d}{dz} \left[\tilde{D}(c) \frac{dc}{dz} \right] + \frac{d^2n}{dz^2} = -v \frac{d}{dz} (c + n).$$

Integrating the result, we obtain the expression:

$$\frac{D}{D_n} \tilde{D}(c) \frac{dc}{dz} + \frac{dn}{dz} = -v(c + n) + \text{const.}$$

The boundary conditions at $\pm\infty$ dictate that the constant of integration is equal to v . Introducing $m = dc/dz$, we rewrite the resulting equation as

$$\frac{D}{D_n} \tilde{D}(c)m + \frac{dn}{dz} = v(1 - c - n).$$

This last equation, Eq. (20), and the definition of m constitute the conservative system of three first-order ODEs:

$$\frac{dc}{dz} = m, \quad (\text{A.3})$$

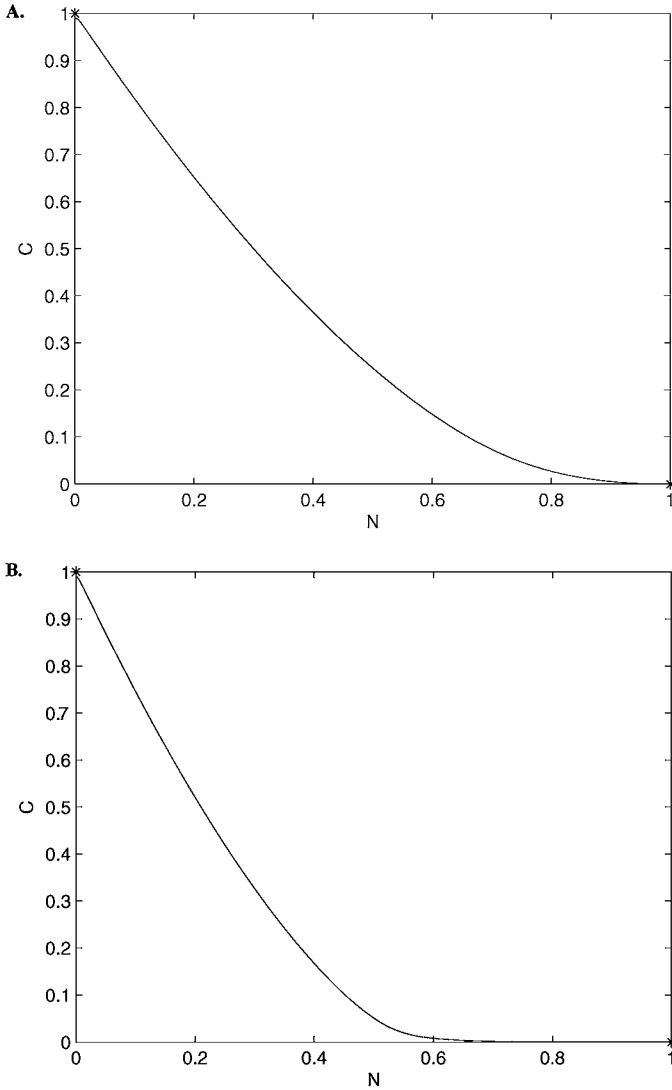


Fig. 7 Phase portrait of the travelling wave ODE system (22–24). The curves show the projections of the heteroclinic trajectories joining two steady states in the 3D phase space onto the $C - N$ -plane for three different values of the traveling wave speed v . A. $v = 2\sqrt{D/D_n}$; B. $v = \sqrt{D/D_n}$; C. $v = 0.5\sqrt{D/D_n}$. The model parameters are $D/D_n = 0.2$, $\epsilon = 0.06$, $c^* = 0.1$.

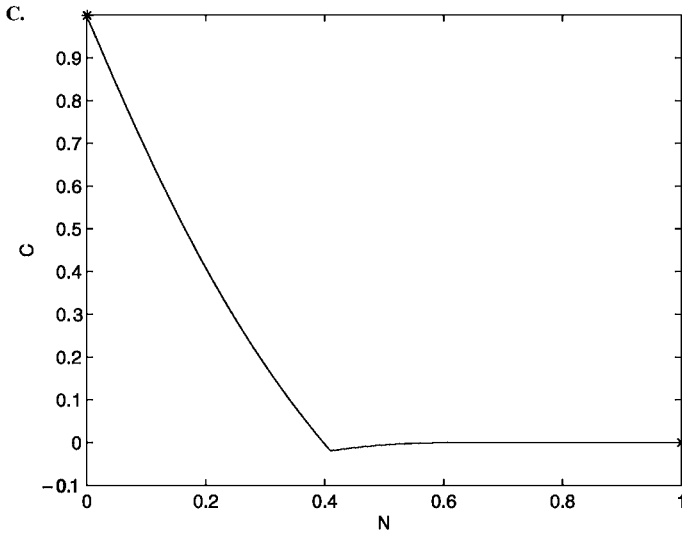


Fig. 7 Continued.

$$\frac{dn}{dz} = v(1 - c - n) - (D/D_n)\tilde{D}m, \tag{A.4}$$

$$\frac{dm}{dz} = -\frac{v}{(D/D_n)\tilde{D}(c)}m - \frac{c}{(D/D_n)\tilde{D}(c)}n - (\ln D)'m^2, \tag{A.5}$$

where $(\ln D)' = d(\ln(\tilde{D}(c)))/dc$.

Any integral curve corresponding to a traveling wave solution must connect two singularities: the initial point $c_v = 1, n_v = 0$ and the final point $c_v = 0, n_v = 1$ (Billingham and Needham, 1991a,b). The initial singularity is an unstable node and the final one is an unstable saddle point. For a given value of v , there is always one integral curve from the infinite set of curves leaving the initial singularity that enters the final singularity. In the 3D phase space, the biologically acceptable solutions must remain positive: $c_v \geq 0, n_v \geq 0$ (Billingham and Needham, 1991a,b).

We found the corresponding curves for numerous values of v, D, ϵ, c^* by solving Eqs. (22–24) numerically. Figures 7A–C (corresponding to $D/D_n = 0.2, \epsilon = 0.06, c^* = 0.1$, and $v = 0.5\sqrt{D/D_n}, \sqrt{D/D_n}$, and $2\sqrt{D/D_n}$) show the projections of three integral curves onto the $c - n$ -plane. These figures illustrate that the solutions corresponding to $v = 2\sqrt{D/D_n}$ and $v = \sqrt{D/D_n}$ are biological, but the solution corresponding to $v = 0.5\sqrt{D/D_n}$ is not. In the latter case $c(z)$ is not always positive. Careful numerical analysis indicates that biologically relevant traveling wave solutions exist for $v \geq \mu(\epsilon, c^*)\sqrt{D/D_n}$, where μ is the same as that in Eq. (19). Therefore, though we do not prove it rigorously here, combined phase plane and numerical analyses indicate that the velocity of the evolving stable traveling wave is equal to the minimal biologically relevant speed, as

in many other similar models (see Billingham and Needham, 1991a,b; Ben-Jacob et al., 2000).

References

- Alber, M.S., Kiskowski, M.A., Jiang, Y., 2004. Two-stage aggregate formation via streams in *myxobacteria*. *Phys. Rev. Lett.* 93, 068102.
- Bees, M.A., Andresen, P., Mosekilde, E., Givskov, M., 2002. Quantitative effects of medium hardness and nutrient availability on the swarming motility of *Serratia liquefaciens*. *Bull. Math. Biol.* 64, 565–587.
- Ben-Jacob, E., Cohen, I., Levine, H., 2000. Cooperative self-organization of microorganisms. *Adv. Phys.* 49, 395–554.
- Ben-Jacob, E., Schochet, O., Tenenbaum, A., Cohen, I., Czirok, A., Vicsek, T., 1994. Generic modelling of cooperative growth patterns in bacterial colonies. *Nature* 368, 46–49.
- Berg, H., Budrene, E., 1991. Complex patterns formed by motile cells in *E. coli*. *Nature* 349, 630–633.
- Berg, H.C., 1993. *Random walks in biology*. Princeton University Press, Princeton, NJ.
- Billingham, J., Needham, D.J., 1991a. The development of traveling waves in quadratic and cubic autocatalysis with unequal diffusion rates. I. Permanent form traveling waves. *Phil. Trans. R. Soc.: Phys. Sci. Eng.* 334, 1–24.
- Billingham, J., Needham, D.J., 1991b. The development of traveling waves in quadratic and cubic autocatalysis with unequal diffusion rates. II. An initial value problem with an immobilized or nearly immobilized autocatalysis. *Phil. Trans. R. Soc.: Phys. Sci. Eng.* 336, 497–539.
- Borner, U., Deutsch, A., Reichenbach, H., Bar, M., 2002. Rippling patterns in aggregates of *myxobacteria* arise from cell–cell collisions. *Phys. Rev. Lett.* 89, 078101.
- Bray, D., 2002. *Cell Movements*. Garland, New York.
- Burchard, R., 1974. Growth of surface colonies of the gliding bacterium *Myxococcus xanthus*. *Arch. Microbiol.* 96, 247–254.
- Deutsch, A., 1995. Towards analyzing complex swarming patterns in biological systems with the help of lattice–gas cellular automata. *J. Biol. Syst.* 3, 947–955.
- Dockery, J.D., Keener, J.P., 2001. A mathematical model for quorum sensing in *Pseudomonas aeruginosa*. *Bull. Math. Biol.* 63, 95–116.
- Dworkin, M., Eide, D., 1983. *Myxococcus xanthus* does not respond chemotactically to moderate concentration gradients. *J. Bacteriol.* 154, 437–442.
- Edelstein-Keshet, L., 1988. *Mathematical Models in Biology*. Random House, New York.
- Esipov, S., Shapiro, D., 1998. Kinetic model of *Proteus mirabilis* swarm colony development. *J. Math. Biol.* 36, 249–268.
- Fife, P.C., 1979. *Mathematical Aspects of Reacting and Diffusing Systems*. Springer, Berlin.
- Garcia, A.L., 2000. *Numerical Methods for Physics*. Prentice-Hall, Englewood Cliffs, NJ.
- Gray, B.F., Kirwan, N.A., 1974. Growth rates of yeast colonies on solid media. *Biophys. Chem.* 1, 204–213.
- Igoshin, O., Mogilner, A., Welsch, R., Kaiser, D., Oster, G., 2001. Pattern formation and traveling waves in *Myxobacteria*: Theory and modeling. *Proc. Natl. Acad. Sci. U.S.A.* 98, 14913–14918.
- Igoshin, O., Welch, R., Kaiser, D., Oster, G., 2004. Waves and aggregation patterns in *Myxobacteria*. *Proc. Natl. Acad. Sci. U.S.A.* 101, 4256–4261.
- Jelsbak, L., Sogaard-Andersen, L., 2000. Pattern formation: Fruiting body morphogenesis in *Myxococcus xanthus*. *Curr. Opin. Microbiol.* 3, 637–642.
- Kaiser, D., Crosby, C., 1983. Cell movement and its coordination in swarms of *Myxococcus xanthus*. *Cell Motil.* 3, 227–245.
- Kawasaki, K., Mochizuchi, A., Matsushita, M., Umeda, T., Shigesada, N., 1997. Modeling spatio-temporal patterns generated by *Bacillus subtilis*. *J. Theor. Biol.* 188, 177–185.
- Koch, A.L., 1999. Diffusion through agar blocks of finite dimensions: A theoretical analysis of three systems of practical significance in microbiology. *Microbiology* 145, 643–654.
- Komoto, A., Hanaki, K., Maenosono, S., Wakano, J.Y., Yamaguchi, Y., Yamamoto, K., 2003. Growth dynamics of *Bacillus circulans* colony. *J. Theor. Biol.* 225, 91–97.
- Lutscher, F., Stevens, A., 2002. Emerging patterns in a hyperbolic model for locally interacting cell systems. *J. Nonlinear Sci.* 12, 619–640.

- Merz, A.J., So, M., Sheetz, M.P., 2000. Pilus retraction powers bacterial twitching motility. *Nature* 407, 98–102.
- Murray, J.D., 1993. *Mathematical Biology*. Springer, Berlin.
- Nagai, T., Ikeda, T., 1991. Traveling waves in a chemotactic model. *J. Math. Biol.* 30, 169–184.
- Newman, W.I., 1980. Some exact solutions to a nonlinear diffusion problem in population genetics and combustion. *J. Theor. Biol.* 85, 325–334.
- Othmer, H.G., Stevens, A., 1997. Aggregation, blowup and collapse: The ABC's of taxis in reinforced random walks. *SIAM J. Appl. Math.* 57, 1044–1081.
- Pfisterer, B., 1989. A one-dimensional model for the swarming behavior of *Myxobacteria*. In: Alt, W., Hoffmann, G. (Eds.), *Biological Motion*. Springer, Berlin, pp. 556–563.
- Rauprich, O., Matsushita, M., Weijer, C.J., Siegert, F., Esipov, S.E., Shapiro, J.A., 1996. Periodic phenomena in *Proteus mirabilis* swarm colony development. *J. Bacteriol.* 178, 6525–6538.
- Rosenberg, E., Keller, K.H., Dworkin, M., 1977. Cell density-dependent growth of *Myxococcus xanthus* on casein. *J. Bacteriol.* 129, 770–777.
- Santoianu, R.A., Maini, P.K., Garduno, F.S., Armitage, J.P., 2001. Traveling waves in a nonlinear degenerate diffusion model for bacterial pattern formation. *Disc. Cont. Dyn. Syst. B* 1, 339–362.
- Shapiro, J.A., 1998. Thinking about bacterial populations as multicellular organisms. *Annu. Rev. Microbiol.* 52, 81–104.
- Shi, W., Kohler, T., Zusman, D.R., 1993. Chemotaxis plays a role in the social behavior of *Myxococcus xanthus*. *Mol. Microbiol.* 9, 601–611.
- Shi, W., Ngok, F.K., Zusman, D.R., 1996. Cell density regulates cellular reversal frequency in *Myxococcus xanthus*. *Proc. Natl. Acad. Sci. U.S.A.* 93, 4142–4146.
- Shimkets, L.J., Kaiser, D., 1982. Induction of coordinated movement of *Myxococcus xanthus* cells. *J. Bacteriol.* 152, 451–461.
- Spormann, A.M., 1999. Gliding motility in bacteria: Insights from studies of *Myxococcus xanthus*. *Microbiol. Mol. Biol. Rev.* 63, 621–641.
- Spormann, A.M., Kaiser, A.D., 1995. Gliding movements in *Myxococcus xanthus*. *J. Bacteriol.* 177, 5846–5852.
- Spormann, A.M., Kaiser, A.D., 1999. Gliding mutants of *Myxococcus xanthus* with high reversal frequencies and small displacements. *J. Bacteriol.* 181, 2593–2601.
- Stevens, A., 1995. Trail following and aggregation of myxobacteria. *J. Biol. Syst.* 3, 1059–1068.
- Ward, M.J., Mok, K.C., Zusman, D.R., 1998. *Myxococcus xanthus* displays Frz-dependent chemokinetic behavior during vegetative swarming. *J. Bacteriol.* 180, 440–443.
- Wolgemuth, C., Hoiczky, E., Kaiser, D., Oster, G., 2002. How myxobacteria glide. *Curr. Biol.* 12, 369–377.
- Woodward, D.E., Tyson, R., Myerscough, M.R., Murray, J.D., Budrene, E.O., Berg, H.C., 1995. Spatio-temporal patterns generated by *Salmonella typhimurium*. *Biophys. J.* 68, 2181–2189.